X-RAY DIFFRACTION ANALYSIS OF SURFACE Si NANOSTRUCTURES USED FOR Ge NANOHETEROEPITAXY

J. Matějová[1,2], G. Kozlowski[1], P. Zaumseil[1], V. Holý[2] and T. Schröder[1]

[1]*IHP, Im Technologiepark 25, D-15236 Frankfurt (Oder), Germany*
[2]*Faculty of Mathematics and Physics, Charles University, Ke Karlovu 5, 121 16 Prague, Czech Republic*
matejova@ihp-microelectronics.com

Keywords:

Ge epitaxy, nanostructured Si, nanoheteroepitaxy, X-ray diffraction

Abstract

The integration of low-defect Ge layers on Si substrate is of increasing interest due to its possible applications in optoelectronics and CMOS technologies. To avoid nucleation of dislocations caused by relatively large lattice mismatch between Si and Ge, nanoheteroepitaxy strain-relieving mechanism was suggested. To prove the functionality of this mechanism, we investigate the strain field in Si line nanostructures covered by SiO_2 growth mask with dimensions in order of 100 nm. By comparison of experimental XRD data with simulations (X-ray kinematical scattering theory), we refined the shape coordinates of the nanostructures (i.e. coordinates of selected points from Si-pillar borderline, between which the borderline can be interpolated by linear function with minor error) taken from TEM images. We carried out a strain field simulation based on the elasticity theory and showed insufficiency of conventional model of the strain in Si after thermal oxidation. Therefore we implemented an iterative evolutionary algorithm to determine the strain field from the experimental XRD data. Preliminary results, where we reached 1 order better agreement, are shown.

Introduction

Growing low-defect Ge layers on Si substrate is of increasing interest nowadays because of its possible application in CMOS technologies and optoelectronics. Nanoheteroepitaxy is a novel approach designed to decrease the elastic lattice misfit energy in Ge layer below the nucleation energy of defects and consequently to reduce the amount of dislocations in Ge layers [1]. The elastic energy reduction can be reached by a deposition of Ge on laterally structured Si substrates containing small zero- or one-dimensional nanostructures (dots or stripes, respectively). Afterwards the accommodation of the lateral Si lattice parameter of the nanostructures to that of the above-deposited Ge lattice provides the strain-relieving mechanism. (See Fig. 1.)

The efficiency of the nanoheteroepitaxy growth is substantially affected by a residual deformation in the Si nanostructures caused by a lithography oxide mask. We have studied this deformation by high-resolution X-ray diffraction analysis. In the presented study we concentrate on one-dimensional line nanostructures along the [110] direction.

Methods

The samples with nanostructured Si pillars were prepared lithographically on a Si(001) substrate in following steps:

1. preparing multilayer system according to Fig. 2,
2. exposure of photoresist to UV-light through a mask,
3. development of the photoresist,
4. wet etching of the hard mask through the remaining photoresist,
5. wet etching of Si substrate through the remaining hard mask.

Thus we obtain a regular grid of structures with lateral periodicity 360 nm. The target height of the pillars is about 150 nm. The growth mask for Ge selective deposition was made by wet thermal oxidation of Si, so that the top-surface of the pillars is free-standing Si and the sidewalls and trenches are covered by SiO_2 and Ge could attach only on the top. (See Fig. 3a and Fig. 3b.) This preparation is based on the gate oxide spacer technique used in IHP 0.13 m BiCMOS technology [2].

The XRD experiments were carried out with a laboratory-based equipment (Rigaku SmartLab) in high-resolution setup with analyzer (Ge(400)×2 collimator, Ge(220)×2 analyzer) and parallel beam condition. We concentrated on symmetric Si (004) diffraction, */2* - and

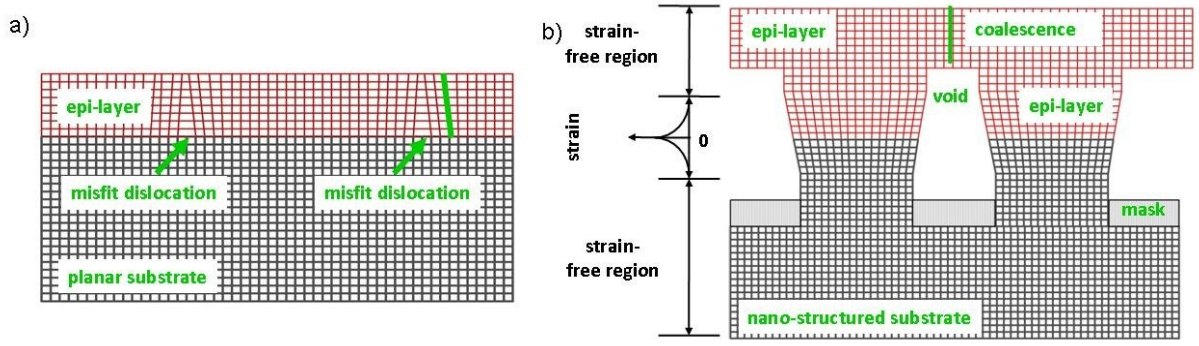

Figure 1. (Based on a picture from the proposal of [1].) Classical planar heteroepitaxy (a) and innovative 3D nanoheteroepitaxy (b) approach of a lattice mismatched epilayer (e.g. Ge) on planar (a) or nanostructured (b) Si(001) substrate.

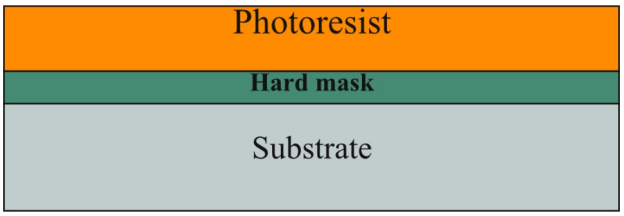

Figure 2. A sketch of multilayer system for lithographical preparation of Si nanopillars.

-scans, first (before investigating full reciprocal space maps).

To analyze the measured data, we worked with two distinct approaches.The first one consists of getting the strain field of the nanostructures by solving the elasticity equations for the particular case of Si pillar and growth mask. This can be achieved by finite-element method. From the strain field, we can directly determine theoretical diffraction curves using kinematical approximation for X-ray scattering from lateral nanostructures [3] and then compare them with experimental data.

The second approach involves an iterative evolution algorithm for determining strain depth-profile from experimental data, while the underlying X-ray scattering theory is the same as in former case.

Results and Discussion

1. Variation of diffraction curves with oxide-layer thickness

Fig. 4 shows diffraction Q_x- and Q_z- scans for various values of thickness of the oxide layer: 30 nm SiO_2, 10 nm SiO_2 and etched sample without the oxide. In Q_x- scan (Fig. 4 - left), one can observe the oscillations due to the lateral periodicity of the samples, whereas in Q_z- scan (Fig. 4 - right), the oscillations due to the finite height of Si pillars are visible. We can also determine the approximate mean value of the nanostructures dimensions according to the equations (1).

$$D \quad 2 / Q_x \qquad (1a)$$

$$c \quad 2 / Q_z \qquad (1b)$$

The results are shown in Tab. 1.

The asymmetry in Q_z-scan is related to strain in the nanostructures, driven by the oxide growth mask. Shoulder of lower Q_z values indicates tensile strain off-plane direction, which results in compressive strain in in-plane (lateral) direction. In Q_x-scan, the strain influences only intensities of satellite maxima and results in no asymmetry, because lateral strain has no impact on diffraction 004.

Moreover, there is evidence that strain in Si nanostructures increases with increasing oxide layer thickness.

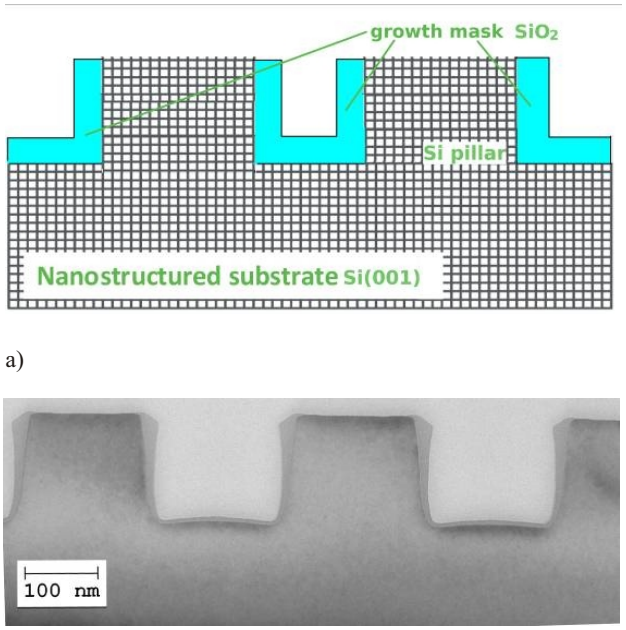

a)

Figure 3. a) A sketch of the samples for presented study. **b)** Cross section TEM image of Si line nanostructures on Si(001), covered by SiO_2 growth mask.

2. Zero-strain case: etched sample

To determine the shape coordinates of the nanostructures, we can yield rough information from TEM images (see for example Fig. 3 and Tab. 1). However, these images give us only local information. Therefore we consider variation of this shape within approx. 100 Å for different pillars of the sample. The comparison of experimental data with simulation of diffracted intensity for unstrained nanostructures provides us detailed geometrical parameters of the pillars, because the diffraction curves are determined only by the shape of the Si pillars.

As the zero strain in the crystal lattice could be supposed, SiO_2 was removed from the sample by etching, Starting coordinates of the shape of Si pillars were taken from TEM images and then refined by fitting the simulated diffraction curve to the experimental one. (See Fig. 5a.) (We suppose, that the shape of Si pillars was not modified by the etching process.) For XRD-based determination of the shape coordinates we estimated almost 2 orders smaller error than for TEM-based one. (See Tab. 1.) Resulting shape coordinates for both methods (including the limits of their error for TEM-based coordinates) are shown in Fig. 5b. The coordinates determined these methods are in agreement within the ranges of estimated errors. Nevertheless, XRD-based determination of the shape is more precise, i.e. with smaller estimated error.

Table 1. Parameters of the nano-pillars determined from TEM vs. from XRD.

	Description	Values determined from a single TEM image	Values determined from diffraction scans
D	lateral period of the nanostructures	(3500 ± 100) Å	(3600 ± 5) Å
c	height of pillar	(1600 ± 100) Å	(1510 ± 5) Å

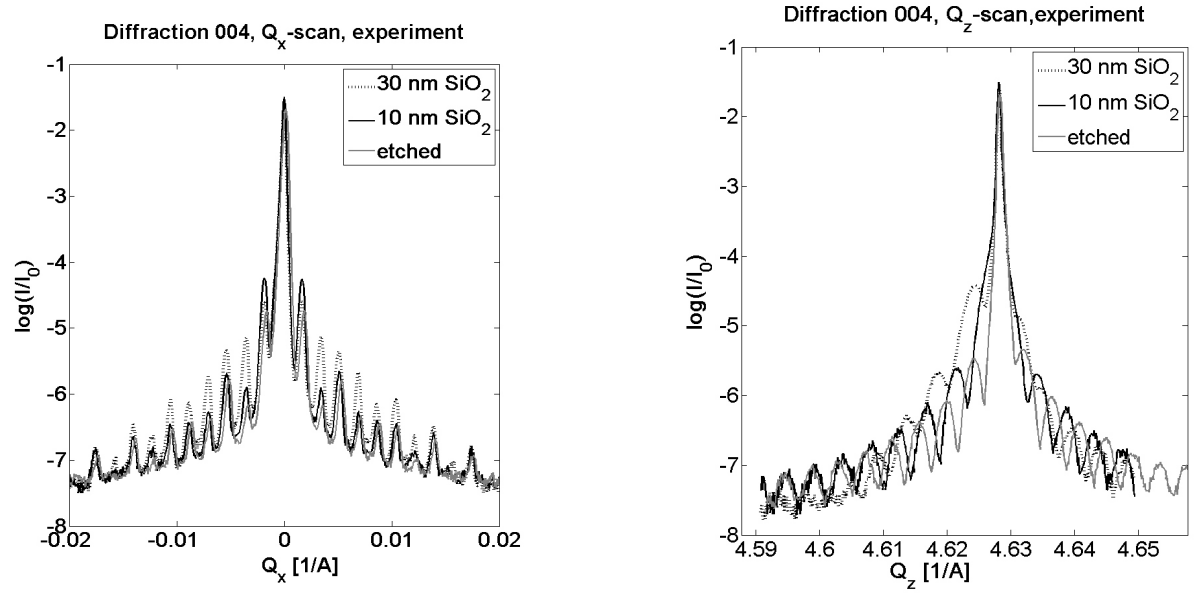

Figure 4. Experimental data for various thicknesses of the oxide layer. Left: Q_x - scan, right: Q_z - scan.

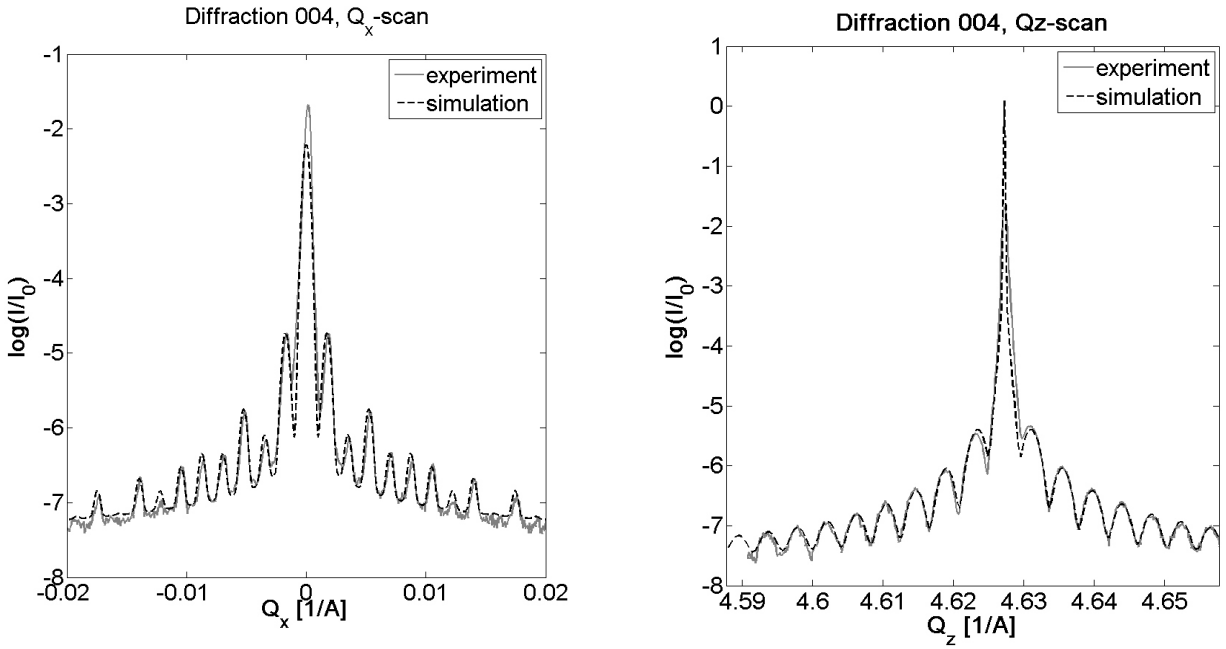

Figure 5a. Experimental curves measured on etched sample vs. simulation with zero strain**.**

3. Direct determination of the diffraction curves from simulated strain field

The strain field in nanostructured sample can be determined by solving equilibrium elasticity equations [4] for particular case of the given structure. In this case, the structure is described by the precise shape of Si pillar and oxide layer and by elasticity parameters of both materials.

The numerical solution was found by finite-element method [5], using the FlexPDE software [6], for one lateral section of the sample. Both right and left boundaries were fixed in the in-plane x direction (i.e. $u_x^{(boundary)} = 0$), so as both periodicity and mirror symmetry were provided. A rigid Si substrate was achieved by the bottom of the domain fixed in z-direction. The substrate thickness was chosen so as its influence on the stress in the nano-patterned pillar would be eliminated. We assumed initial stress conditions

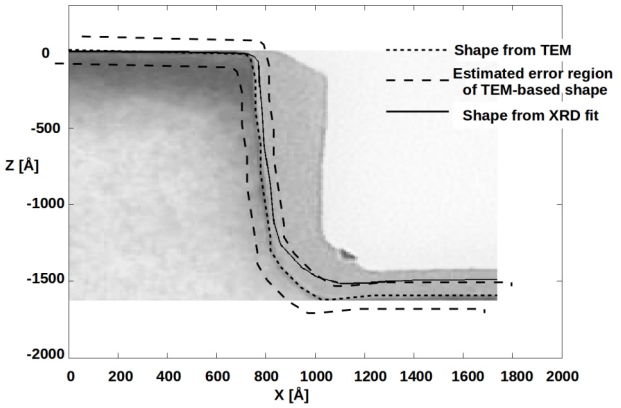

Figure 5b. The shape coordinates of the Si pillar determined from TEM (short-dashed line) vs. by fitting XRD scans (solid line). Background TEM image depicts Si nanopillar covered by SiO_2.

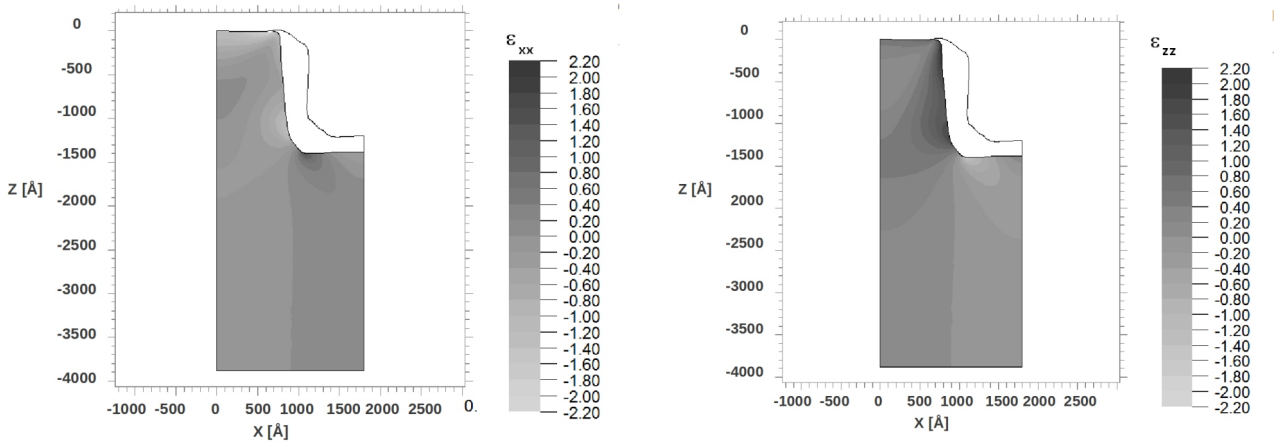

Figure 6. FEM-simulated strain field. Left: in-plane strain $\varepsilon_{xx}(x,z)$, right: off-plane strain $\varepsilon_{zz}(x,z)$. The scale corresponds to $f = 1$.

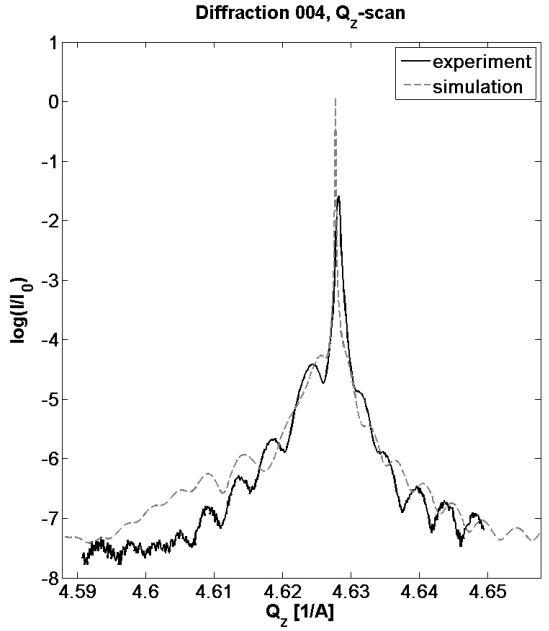

Figure 7. Comparison of experimental Q_z-scan with the FEM-simulation based one – the best fit with $f = 13$, whereas merit function **MF = 0.5**.

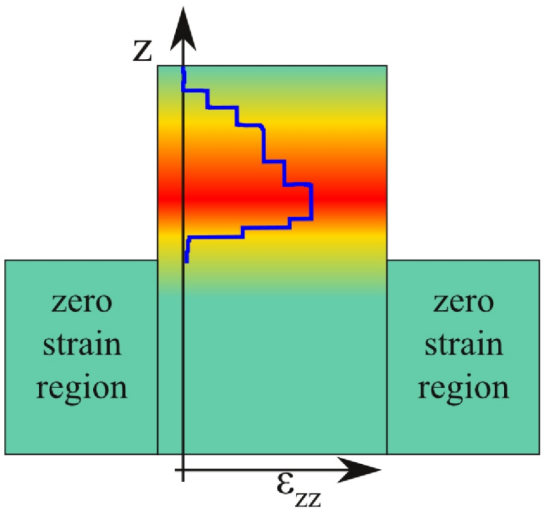

Figure 8. Sketch of the first-step simple strain model.

with a free parameter f, which can be yielded by fitting the simulated diffraction scans to the experimental ones. Equations (2a,b) interconnect fitted strain fields $\varepsilon_{xx}^{(fitted)}$, $\varepsilon_{zz}^{(fitted)}$ with the ones simulated for $f = 1$, i.e. ε_{xx}, ε_{zz}.

$$\varepsilon_{xx}^{(fitted)} \quad f \quad \varepsilon_{xx} \qquad (2a)$$

$$\varepsilon_{zz}^{(fitted)} \quad f \quad \varepsilon_{xx} \qquad (2b)$$

The resulting simulated strain fields ε_{xx}, ε_{zz} are plotted in Fig. 6. (The scale corresponds to $f = 1$.) Consequent computation of diffraction curves was carried out according to the kinematical theory of diffuse X-ray scattering from laterally strained nanostructures [3]. Numerical implementation of this theory includes integration by FFT method with corrections according to [7].

The best fit of XRD Q_z-scan, obtained by this approach, in comparison with the experimental one can be seen in Fig. 7. To quantify the agreement between the curves, we introduced *merit function* MF by formula (3).

$$MF \quad \frac{1}{N} \sum_{j=1}^{N} (\log_{10}(I^*_{\exp}) \quad \log_{10}(I^*_{calc})), \qquad (3)$$

where N is sampling frequency for the curves comparison, I^*_{exp} is experimental intensity and I^*_{comp} is computed intensity, both normalized to the incident beam.

As the agreement is insufficient, we had to suggest another strategy, which would lead to better results and would serve for analysis of the failure's causes.

Iterative evolutionary algorithm: the simplest strain model

As we have seen, the diffraction curves based on FEM-simulated strain field cannot fit the experimental data by adjusting only one free parameter i.e. scaling factor f. Therefore we suggested a simple model with more free parameters to fit.

In the first step we started with the model sketched in Fig. 8. Constant-strain lamellae are supposed to be in the pillar region and zero strain in the trench areas. In this approach, we supposed 7 constant-strain lamellae and fitted their width, while zero width is also possible. For fitting so many parameters, the method 'trial-error' is not sufficient.

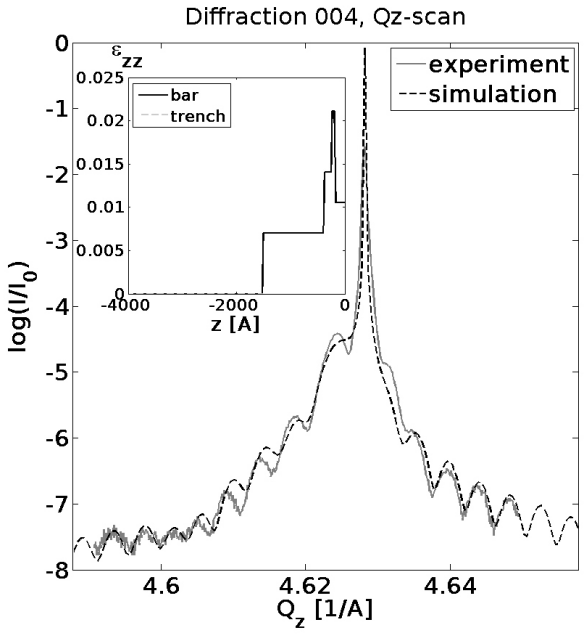

Figure 9. Comparison of experimental Qz-scan with the simulated one (best fit) for the simple model from Fig. 8. Detail: Corresponding strain field. Error function **MF = 0.04**.

That's why the iterations in this algorithm are driven by an evolutionary method [8], while the path from strain field towards diffraction curve remains the same as in the direct approach. We supposed the same shape of the pillars as we got by fitting diffraction curves for the unstrained sample (see Fig. 5b). Preliminary resulting fitted strain profile as well as corresponding Q_z-scan are shown in Fig. 9, while further improvement is required in the form of more complex strain models. Nevertheless, even for this very simple model, we obtain 1 order better agreement with the experiment by this method (see Tab. 2).

Summary and conclusion

From comparison of experimental diffraction scans for various thicknesses of growth mask (Fig. 4), we deduced, that strain in Si nanostructures increases with increasing oxide layer thickness. By determining strain character, we found that growth mask would suppress the strain relieving mechanism, when Ge epilayer would be deposited on top.

We also deduced precised geometry of nanostructures by comparing experimental data measured on etched samples with the simulation for zero strain.

Furthermore, we carried out a simulation of the strain field in the nanostructures as a solution of elasticity equations by FEM. Subsequently, we computed the diffracted intensity based on this strain field. Thus obtained Q_z-scan is not in agreement with experimental data, which implies, that the elasticity model or its parameters are not precise enough.

Table 2. Comparison of merit functions of Q_z-scans for direct simulation vs. iterative simulation.

Direct FEM-based simulation	MF(FEM)=0.5
Iterative simulation	MF(ITER)=0.04

Therefore we introduced an iterative evolutionary algorithm for determining strain field from X-ray diffraction curve. Preliminary results (the simplest first-step model from Fig. 8) are shown in Fig. 9, while further improvement is required. It can be achieved by dividing the pillar into more constant-strain areas also at in-plane direction.

Acknowledgements

We acknowledge Y. Yamamoto and J. Bauer for samples preparation and A. Schubert for taking TEM images.

References

1. D. Zubia, S.H. Zaidi, S.D. Hersee & S.R. Brueck, *J. Vac. Sci. Technolog. B*, **18**, (2000), 3514-3520.
2. H. Rücker, B. Heinemann, W. Winkler, R. Barth, J. Borngräber, J. Drews, G.G. Fischer, A. Fox, T. Grabolla, U. Haak, D. Knoll, F. Korndörfer, A. Mai, S. Marschmeyer, P. Schley, D. Schmidt, J. Schmidt, K. Schultz, B. Tillack, D. Wolansky & Y. Yamamoto, *Proceedings IEEE BCTM*, (2009), 166.
3. U. Pietsch, V. Holy & T. Baumbach, *High-Resolution X-Ray Scattering*. New York: Springer - Verlag. 2004.
4. H. Ibach, *Physics of Surfaces and Interfaces*. Berlin: Springer –Verlag. 2006.
5. K.-J. Bathe, *Finite Element Method*. John Wiley & Sons, Inc. 2007.
6. FlexPDE, PDE Solutions Inc.: `http://www.pdesolutions.com/`
7. W.H. Press, S.A. Teukolsky, W.T. Vitterling & B.P. Flannery, *Numerical Recipes*. New York: Cambridge University Press. 1986.
8. T. Bäck, *Evolutionary Algorithms in Theory and Practice*. Oxford: Oxford Univ. Press.1996.